

The “Main Sequence” of Explosive Solar Active Regions: Discovery and Interpretation

Short Title: “Main Sequence” of Explosive Solar Active Regions

David A. Falconer^{1,2,3}, Ronald L. Moore¹, G. Allen Gary³, and Mitzi Adams¹

¹ Space Science Office, VP62, Marshall Space Flight Center, Huntsville, AL 35812

² Physics Department, University of Alabama in Huntsville, Huntsville, AL 35899

³ Center for Space Plasma and Aeronomic Research, University of Alabama in Huntsville,
Huntsville, AL 35899

Email Address of Corresponding Author: David.falconer@msfc.nasa.gov

We examine the location and distribution of the production of coronal mass ejections (CMEs) and major flares by sunspot active regions in the phase space of two whole-active-region magnetic quantities measured from 1897 SOHO/MDI magnetograms. These magnetograms track the evolution of 44 active regions across the central disk of radius $0.5 R_{\text{Sun}}$. The two quantities are ${}^L\text{WL}_{\text{SG}}$, a gauge of the total free energy in an active region’s magnetic field, and ${}^L\Phi$, a measure of the active region’s total magnetic flux. From these data and each active region’s history of production of CMEs, X flares, and M flares, we find (1) that CME/flare-productive active regions are concentrated in a straight-line “main sequence” in ($\text{Log } {}^L\text{WL}_{\text{SG}}$, $\text{Log } {}^L\Phi$) space, (2) that main-sequence active regions have nearly their maximum attainable free magnetic energy, and (3) evidence that this arrangement plausibly results from equilibrium between input of free energy to an explosive active region’s magnetic field in the chromosphere and corona by contortion of the field via convection in and below the photosphere and loss of free energy via CMEs, flares, and coronal heating, an equilibrium between energy gain and loss that is analogous to that of the main sequence of hydrogen-burning stars in (Mass, Luminosity) space.

Key words: Sun: magnetic fields – Sun: coronal mass ejections (CMEs) – Sun: flares

1. INTRODUCTION

For an active region’s chromospheric and coronal magnetic field to be able to explode in a CME/flare eruption, it should have enough free magnetic energy, at least as much as is consumed by the eruption (e.g., Gopalswamy et al 2006). That is, the active region should have enough magnetic field and the field should be deformed enough from its potential-field configuration, the minimum-energy configuration in which there is no free energy. Indeed, it is observationally well established that the CME/flare productivity of active regions increases with both the nonpotentiality and the magnetic size of the active region, the nonpotentiality being the overall degree of nonpotential shear/twist in the active region’s magnetic field and the magnetic size being the active region’s flux content (its total magnetic flux) (e.g., Canfield et al 1999; Falconer et al 2002, 2006). The product of any measure of the nonpotentiality and the flux content is a free-energy-content measure, a gauge of the total free energy in the active region’s magnetic field (the active region’s free-magnetic-energy content). Conversely, any free-energy-content measure divided by the active region’s flux content is a gauge of the nonpotentiality of the active region’s field (Falconer et al 2006). Consistent with these relations, we found from

measurement of vector magnetograms of strong-field active regions that active-region CME/flare productivity is more strongly correlated with free-energy-content measures than with either nonpotentiality measures alone or the flux content alone (Falconer et al 2006). But this result was puzzling in that it implied that of two active regions having magnetic fields of the same nonpotentiality but different flux content, the active region of larger flux content is more likely to produce a CME/flare eruption than is the active region of smaller flux content. The physical reason for this tendency was not obvious, at least to us. Partly in response to this puzzle, we conjectured that further insight to the magnetic causes of the CME/flare productivity of active regions might be gained by examining the location and distribution of CME/flare-productive active regions in the two-dimensional phase space of active-region free magnetic energy and active-region magnetic size. In this Letter, we present a first look at CME/flare-productive active regions from this perspective.

2. DATA

The data that we use to obtain our new perspective are paired values of two whole-active-region magnetic quantities measured from active-region magnetograms cropped from SOHO/MDI full-disk magnetograms that had the most recent calibration (Level 1.8.2). The two magnetic quantities are a free-energy-content measure, denoted by ${}^L W_{LSG}$, and a flux-content measure, denoted by ${}^L \Phi$. For each of 44 active regions, we measured these two quantities from each MDI magnetogram of the active region taken during the active region's passage within 30 heliographic degrees from disk center. The 96-minute cadence of the MDI magnetograms yielded a total of 1897 measured active-region magnetograms. In $({}^L W_{LSG}, {}^L \Phi)$ space, the sequence of measured values for each active region is a track displaying the active region's evolution in free-energy content and flux content during the few-day interval in which the Sun's rotation carried the active region across the $0.5 R_{Sun}$ central disk. It is the continuity and cadence of the MDI magnetograms, together with each active region's history of production of CMEs and flares during its central disk passage, that deliver the new perspective on the free magnetic energy and magnetic size of CME/flare-productive active regions.

Because MDI magnetograms are line-of-sight magnetograms, ${}^L W_{LSG}$ and ${}^L \Phi$ are measured from the line-of-sight component of the active region's magnetic field. For any active region not right at disk center, ${}^L W_{LSG}$ and ${}^L \Phi$ are approximations of the corresponding measures, W_{LSG} and Φ , that would be measured from the vertical-field component of a vector magnetogram of the active region, once the magnetogram were deprojected to disk center, so that it showed the active region as if it were viewed directly from above. The way that each of these four measures is measured from an active-region magnetogram and the way the uncertainty in the measurement is estimated are described in Falconer et al (2006) and Falconer et al (2008). The free-energy-content measure W_{LSG} is the gradient-weighted integral length of strong-field neutral line in the active region. It is a measure of the free-magnetic-energy content by virtue of the horizontal gradient of the vertical field at strong-field neutral lines in active regions being closely correlated with the shear in the horizontal field at these neutral lines (Falconer et al 2003, 2006, 2008). W_{LSG} is the line integral of the vertical-field horizontal gradient over all strong-field intervals of the neutral lines in the deprojected vector magnetogram [$W_{LSG} = \int |\nabla B_z| dl$, where ∇B_z is the horizontal gradient of the vertical magnetic field, and a strong-field interval of a neutral line is one on which the horizontal component of the potential field computed from the vertical-field component of the deprojected vector magnetogram is >150 G]. The flux-content measure Φ is

the total unsigned vertical-field magnetic flux stronger than 100 G in the deprojected vector magnetogram of the active region [$\Phi = \int |B_z| dA$, where $|B_z|$ is the strength of the vertical field in the deprojected vector magnetogram and the integral is over all areas of the magnetogram in which $|B_z| > 100$ G]. The free-energy-content measure ${}^L\text{WL}_{\text{SG}}$ and the flux-content measure ${}^L\Phi$ are the approximations of WL_{SG} and Φ obtained from a line-of-sight magnetogram of the active region [${}^L\text{WL}_{\text{SG}} = \int |\nabla B_{\text{los}}| dl$, where ∇B_{los} is the transverse gradient of the line-of-sight magnetic field and the integral is the line integral over all neutral-line intervals on which the potential transverse field computed from the magnetogram is > 150 G; ${}^L\Phi = \int |B_{\text{los}}| dA$, where the integral is over all areas of the magnetogram in which $|B_{\text{los}}| > 100$ G]. The 100 G and 150 G threshold values are convenient levels set by the 2σ noise levels of MSFC vector magnetograms (Falconer et al 2006, 2008).

As was each of our previous studies of the relation of active-region nonpotentiality and magnetic size to active-region CME productivity (Falconer 2001; Falconer et al 2002, 2003, 2006, 2008), the present study is limited to active regions that we determined to be strong-field active regions. We deem an active region to be a strong-field active region if the total length of strong-field neutral line is comparable to the linear span of the active region. Practically all strong-field active regions have substantial sunspots. The specific strong-field criterion met by the active regions in the present study is that the active region had $L_S > 0.75 L_{\text{AR}}$, where L_S is the length of strong-field neutral line in a deprojected vector magnetogram of the active region and L_{AR} is the square root of the magnetogram's area in which $|B_z| > 100$ G (Falconer et al 2008). For strong-field active regions observed within 30° of disk center, we have found that projection effects are small enough that ${}^L\text{WL}_{\text{SG}}$ and ${}^L\Phi$ measured from the line-of-sight component of the non-deprojected vector magnetogram each approximates its counterpart (WL_{SG} or Φ) measured from the vertical-field component of the deprojected vector magnetogram to within about a factor of 2 or less, and each correlates with active-region CME productivity as strongly as does its counterpart (Falconer et al 2006, 2008). This performance of ${}^L\text{WL}_{\text{SG}}$ and ${}^L\Phi$ is our basis for using ${}^L\text{WL}_{\text{SG}}$ and ${}^L\Phi$ measured from MDI line-of-sight magnetograms of strong-field active regions within $0.5 R_{\text{sun}}$ of disk center to examine the evolution and distribution of strong-field active regions in (free-energy content, flux content) phase space.

The set of 44 active regions in the present study is a subset of the 56 strong-field active regions that we measured from Marshall Space Flight Center vector magnetograms in Falconer et al (2008), the 44 that had MDI coverage and were at least a few days old when they rotated onto the $0.5 R_{\text{Sun}}$ central disk. These occurred in the period from 1996 Nov through 2003 Oct. Two other active regions of the 56 had MDI coverage but were not included in the present study because they were born on the central disk, and during their birth phase of rapid emergence, until they were about 2 days old, had markedly different location and evolution in $({}^L\text{WL}_{\text{SG}}, {}^L\Phi)$ phase space than did the 44 more mature active regions. The 44 non-infant strong-field active regions were selected for the present initial study of the CME and flare productivity of active regions in $({}^L\text{WL}_{\text{SG}}, {}^L\Phi)$ phase space not only for their coverage in MDI magnetograms but also because we already had in hand from the Falconer et al (2008) study each active region's CME production history, which we had compiled from the online SOHO LASCO CME catalog (Yashiro et al 2004) and full-Sun coronal movies from Yohkoh/SXT. For the present study, using the NOAA Catalog of Active Region Flares together with the GOES continuous record of 1-8 Å solar X-ray flux and full-Sun coronal movies from Yohkoh/SXT and SOHO/EIT, we have also compiled each active region's history of production of GOES M class and X class flares during the region's disk passage. So, for each active region, we have the starting time of each CME, each

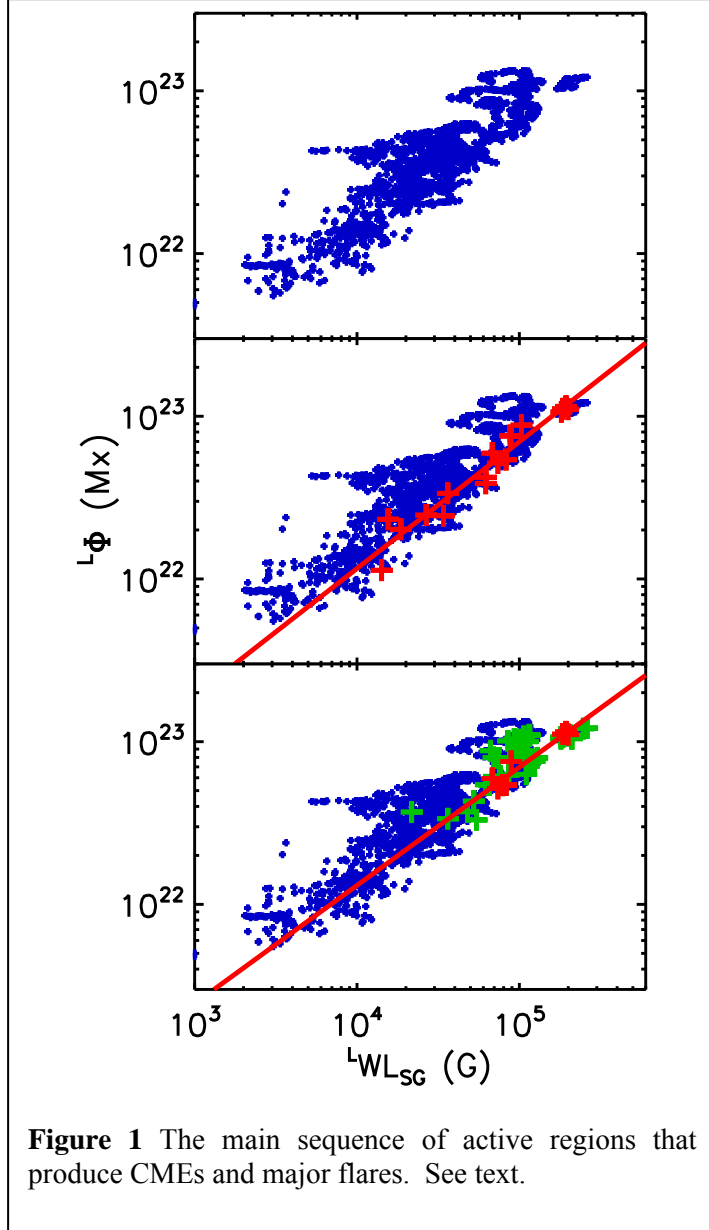


Figure 1 The main sequence of active regions that produce CMEs and major flares. See text.

M flare, and each X flare produced, and from the MDI magnetogram closest to each starting time we have the active region's free-energy-content measure ${}^LW_{LSG}$ and flux-content measure ${}^L\Phi$ when it produced that CME, M flare, or X flare. This information for all 44 active regions gives the location and distribution of these active regions in $({}^LW_{LSG}, {}^L\Phi)$ phase space when they were producing their CMEs and flares.

3. DISCOVERY

The cloud of $({}^LW_{LSG}, {}^L\Phi)$ points (small blue plus signs) obtained by measuring ${}^LW_{LSG}$ and ${}^L\Phi$ from each of the 1897 MDI magnetograms for our 44 active regions is shown in the top panel of Figure 1. The span of each blue plus is somewhat larger than the uncertainty in the measurements. In this Log-Log plot, the cloud loosely covers an oblong diagonal region. Roughly horizontal tracks of some of the active regions that evolved in free-energy content while staying much more nearly constant in flux content are noticeable, especially on the trailing, smaller-free-energy side of the cloud. While evolutionary tracks make the cloud's trailing side ragged and intermittent, the leading edge on the larger-free-energy side of the cloud is

relatively sharp and straight, forming a front having a slope of about $\frac{3}{4}$. The roughly factor-of-ten horizontal width of the cloud in any factor-of-two interval of flux content merely shows that active regions of nearly the same flux content vary widely in free-energy content. The surprise is that the cloud has the rather sharp front and no points of greater free energy much beyond it. From this aspect of the cloud, we infer that for active regions of any one magnetic size there is a maximum attainable free magnetic energy, and that this upper limit steadily increases with magnetic size, the corresponding upper limit on the free-energy-content measure ${}^LW_{LSG}$ increasing with magnetic size roughly as ${}^L\Phi^{4/3}$.

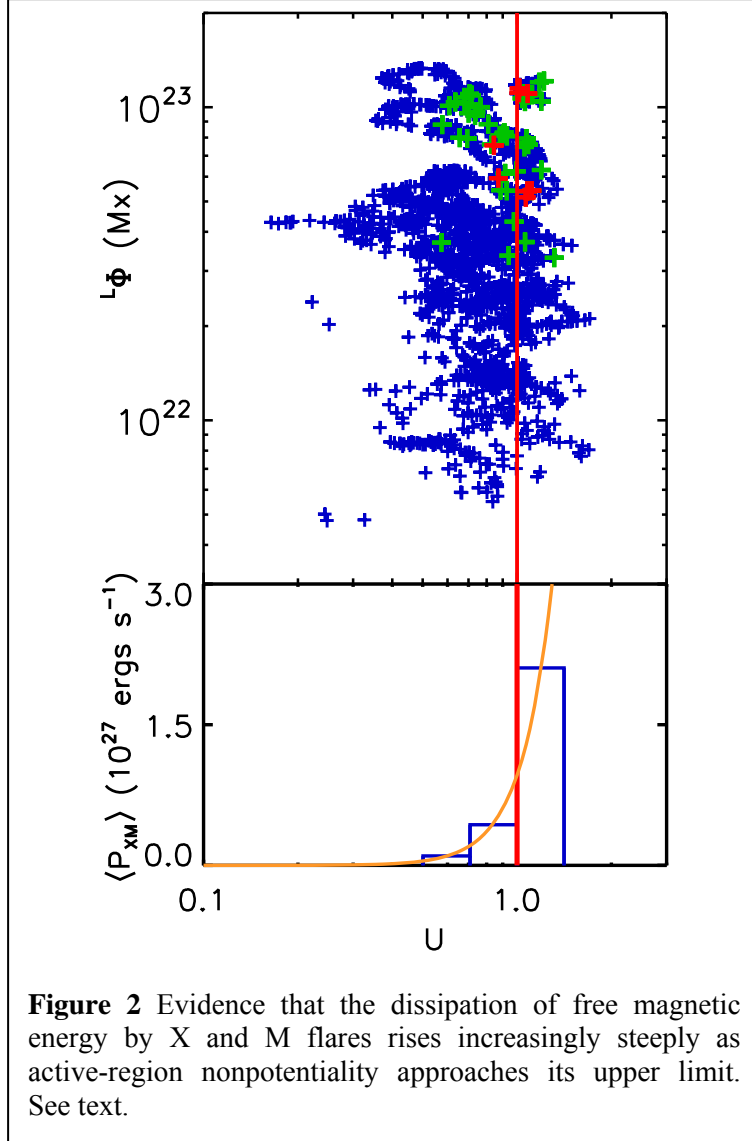
The middle and bottom panels of Figure 1 show that the active regions produced CMEs and X flares only when they were near the cloud's diagonal front, that is, only when they had nearly their maximum attainable free magnetic energy. In the middle panel, for each CME produced by an active region while the active region was within 30° of disk center, the active region's

(${}^L W_{LSG}$, ${}^L \Phi$) point for its magnetogram that was closest in time to the start of the CME's eruption is marked by a red plus sign. The CME points show that CMEs occurred only in active regions near the front edge of the cloud, and only in active regions having magnetic flux within about a factor of 10 of the largest in our sample, or equivalently, only in those having more than about twice the flux of the smallest active region in our sample. The least-squares fit to the CME points runs along the cloud's front, having a slope (0.78) that is about that of the front. In the bottom plot, for each X or M flare produced by our active regions while on the 30° central disk, each flaring active region's magnetogram closest in time to the start of the flare is marked by a red plus sign for an X flare or by a green plus sign for an M flare. The X-flare points show that X flares were produced only by large active regions, those having flux content within about a factor of 3 of that of the largest in our sample, and only when these active regions had close to their maximum attainable free magnetic energy. The M-flare points show that M flares were produced only by active regions having flux content within about a factor of 5 of that of the largest in our sample. The M-flare points also cluster along the front, but scatter farther behind the front than do the X-flare points. The least-squares fit to the X-flare points has a slope (0.73) close to that of the least-squares fit to the CME points and runs along the cloud's front in the same manner. Thus, the data plotted in Figure 1 show that when full-grown active regions produce CMEs and major flares, they populate a "main sequence" in free magnetic energy and magnetic size, a sequence on which the active regions have about their maximum attainable free magnetic energy.

4. INTERPRETATION

The results shown in Figure 1 suggest to us that the free-energy upper-limit front and the accompanying main sequence of explosive active regions are the consequence of the rate of burning down of an active region's free magnetic energy by CMEs, flares, and coronal heating increasing steeply with increasing nonpotentiality of the magnetic field in active regions near the limit, so that on the main sequence there is a rough balance between the burn-down rate and the maximum rate at which free magnetic energy can be built up in the active region. That is, we infer from Figure 1 that the main sequence of explosive active regions is analogous to the main sequence of hydrogen-burning stars in (Mass, Luminosity) space, in that the sequence is a consequence of a rate of energy input being balanced by a rate of energy loss. In this analogy, an active region's gain of free magnetic energy from contortion of its magnetic field by convection in and below the photosphere corresponds to a star's gain of thermal energy from fusion of hydrogen in its core, and the active region's dissipation of its free magnetic energy via magnetic explosions and coronal heating corresponds to a star's loss of thermal energy via its luminosity.

To test the plausibility of our idea that equilibrium between buildup and burn-down of free magnetic energy is the basic condition that produces the main sequence of explosive active regions, we have devised an empirical gauge of an active region's free-energy burn-down rate. This quantity, which we call the active region's flare-power measure and denote by P_{XM} , is a measure of an active region's average rate of dissipation of free energy by X and M flares during a time window centered on a given time. We use 48 hr for the span of the time window. From the NOAA Catalog of Active Region Flares we obtain the active region's history of production of X and M flares and the energy output of each flare in 1-8 Å radiation, the band observed by GOES. The active region's flare-power measure P_{XM} at any given time is this energy output from its X and M flares in the 48 hr interval centered on that time, divided by 48 hr. In this way,



for each of 43 of our 44 active regions, we have evaluated P_{XM} at the time of each of the active region's magnetograms in our sample of 1897 active-region magnetograms. The one omitted active region (AR 7999 of 1996 Nov) is the only one that occurred before the 1997 start of the NOAA Catalog of Active Region Flares.

The distribution of flare points in the bottom plot of Figure 1 appears to indicate that, for active regions large enough to produce X and/or M flares, flare power increases with increasing nearness to the front. To quantify this trend by means of our flare-power measure P_{XM} , we transform the cloud of magnetogram points from the $(\text{Log } {}^L\text{WLSG}, \text{Log } {}^L\Phi)$ space of the plots in Figure 1 to $(\text{Log } U, \text{Log } {}^L\Phi)$ space, where the new coordinate $\text{Log } U$ is perpendicular to the CME least-squares-fit line and increases with increasing active-region nonpotentiality: $U \equiv U_0({}^L\text{WLSG})^{0.78}/{}^L\Phi$, where U_0 is chosen so that $U \equiv 1$ on the CME line. Because $({}^L\text{WLSG})^{0.78}$, like ${}^L\text{WLSG}$, is a free-energy-content measure, U , being

this measure divided by ${}^L\Phi$, is a measure of an active region's nonpotentiality, a gauge of the overall twist in an active region's magnetic field.

The bottom plot in Figure 1 transformed to $(\text{Log } U, \text{Log } {}^L\Phi)$ space is shown in the top plot in Figure 2. In the transformed plot, the maximum-attainable-nonpotentiality front of the cloud is now vertical, and the main sequence of active regions that produced major flares is traced by the $U \equiv 1$ vertical red line close behind the front. The bottom panel of Figure 2 shows a histogram based on only those magnetogram points that had magnetic size ${}^L\Phi$ at or above the smallest ${}^L\Phi$ value of the flare points, that is, above about 4×10^{22} Mx. The bin width is 0.15 in $\text{Log } U$, and the value of $\langle P_{XM} \rangle$ in each bin is the average P_{XM} value of the magnetogram points in that bin. The orange curve is the power law given by least-squares fitting a power law to the histogram: $\langle P_{XM} \rangle \propto U^{4.4}$. The histogram and its power-law fit establish that the rate of dissipation of active-region free magnetic energy by X and M flares rises increasingly steeply with nearness to the nonpotentiality-upper-limit front of the cloud. On the basis of this result, we conclude that the abrupt upper limit on active-region nonpotentiality and the accompanying main sequence of explosive active regions are likely the result of the input of free magnetic energy in active

regions near the front being balanced by the depletion of free magnetic energy by the production of CMEs, flares, and coronal heating.

Figures 1 and 2 together show that a strong requirement for an active region to produce a CME or major flare is that the nonpotentiality U of its magnetic field be at least ~ 1 , and that, conversely, active regions, large or small, having U less than ~ 1 are very unlikely to produce a CME or major flare. These plots also show that along the main sequence of explosive active regions, in addition to U being ~ 1 , the magnetically larger active regions are more productive of CMEs and major flares than are the smaller ones: active regions near the bottom of the $^L\Phi$ range produce few or no CMEs or major flares. This trend was anticipated in the Introduction. We conjecture from these plots that (1) the reason for this trend is that in the smaller active regions near the front the maximum rate of buildup of free energy in the field in the chromosphere and corona by convection in and below the photosphere is usually balanced by small flares and coronal heating and that this dissipation prevents nearly all small active regions from acquiring enough free energy to produce a large CME or major flare, and (2) as active-region magnetic size increases, the balance can only be attained by the addition of increasingly larger magnetic explosions.

This work was supported by funding from NASA's Heliophysics Division, from NSF's Division of Atmospheric Sciences, and AFOSR'S MURI Program.

REFERENCES

- Canfield, R. C., Hudson, H. S., & McKenzie, D. E. 1999, *Geophys. Res. Lett.*, 26, 627.
Falconer, D. A. 2002, *J. Geophys. Res.*, 106, 25185.
Falconer, D. A., Moore, R. L., & Gary, G. A. 2002, *ApJ*, 569, 1016.
Falconer, D. A., Moore, R. L., & Gary, G. A. 2003, *J. Geophys. Res.*, 108, 1380.
Falconer, D. A., Moore, R. L., & Gary, G. A. 2006, *ApJ*, 644, 1258.
Falconer, D. A., Moore, R. L., & Gary, G. A. 2008, *ApJ*, 689, 1433.
Gopalswamy, N., Mewaldt, R., & Torsti, J. 2006, *Solar Eruptions and Energetic Particles* (Washington, DC: AGU).
Yashiro, S., Gopalswamy, N., Michalek, G., St. Cyr, O. C., Plunkett, S. R., Rich, N. B., & Howard, R. A. 2004, *J. Geophys. Res.*, 109, A07105.